JBC Papers in Press. Published on April 14, 2017 as Manuscript M117.787754
The latest version is at http://www.jbc.org/cgi/doi/10.1074/jbc.M117.787754



# Isolation and characterization of a thermostable $F_{420}$:NADPH oxidoreductase from *Thermobifida fusca*

Hemant Kumar,[1,#] Quoc-Thai Nguyen,[1,2,3,#] Claudia Binda,[4] Andrea Mattevi,[4] and Marco W. Fraaije[1]

[1] Molecular Enzymology Group, Groningen Biomolecular Sciences and Biotechnology Institute, University of Groningen, Nijenborgh 4, 9747 AG Groningen, The Netherlands.
[2] Scuola Universitaria Superiore IUSS Pavia, Piazza della Vittoria 15, 27100 Pavia, Italy
[3] Faculty of Pharmacy, University of Medicine and Pharmacy, Ho Chi Minh City, 41 Dinh Tien Hoang Street, Ben Nghe Ward, District 1, Ho Chi Minh City, Vietnam
[4] Department of Biology and Biotechnology, University of Pavia, Via Ferrata 1, 27100 Pavia, Italy

[#] These authors contributed equally to this work
To whom correspondence should be addressed: Prof. dr. M.W. Fraije, Molecular Enzymology Group, Groningen Biomolecular Sciences and Biotechnology Institute, University of Groningen, Nijenborgh 4, 9747 AG Groningen, The Netherlands. Tel: +31503634345. Email: m.w.fraaije@rug.nl.

**Keywords**: *Thermobifida fusca*, $F_{420}$, deazaflavoenzymes, oxidoreductase, nicotinamide adenine dinucleotide phosphate

Running title: $F_{420}$:NADPH oxidoreductase from *T. fusca*

Abbreviations used: FNO, $F_{420}$:NADPH oxidoreductase; Tfu, *Thermobifida fusca*; Af, *Archaeoglobus fulgidus*; NAD(P)$^+$, nicotinamide adenine dinucleotide (phosphate)

## Abstract

$F_{420}H_2$-dependent enzymes reduce a wide range of substrates that are otherwise recalcitrant to enzyme-catalyzed reduction, and their potential for applications in biocatalysis has attracted increasingly attention. *Thermobifida fusca* is a moderately thermophilic bacterium and holds high biocatalytic potential as a source for several highly thermostable enzymes. We report here on the isolation and characterization of a thermostable $F_{420}$:NADPH oxidoreductase (Tfu-FNO) from *T. fusca*, being the first $F_{420}$-dependent enzyme described from this bacterium. Tfu-FNO was heterologously expressed in *Escherichia coli*, yielding up to 200 mg recombinant enzyme per liter of culture. We found that Tfu-FNO is highly thermostable, reaching its highest activity at 65 °C and that Tfu-FNO is likely to act *in vivo* as an $F_{420}$ reductase at the expense of NADPH, similar to its counterpart in *Streptomyces griseus*. We obtained the crystal structure of FNO in complex with NADP$^+$ at 1.8 Å resolution, providing the first bacterial FNO structure. The overall architecture and NADP$^+$-binding site of Tfu-FNO were highly similar to those of the *Archaeoglobus fulgidus* FNO (Af-FNO). The active site is located in a hydrophobic pocket between an N-terminal dinucleotide-binding domain and a smaller C-terminal domain. Residues interacting with the 2′-phosphate of NADP$^+$ were probed by targeted mutagenesis, indicating that Thr28, Ser50, Arg51, and Arg55 are important for discriminating between NADP$^+$ and NAD$^+$. Interestingly, a T28A mutant increased the kinetic efficiency more than three-fold as compared with the wild-type enzyme when NADH is the substrate. The biochemical and structural data presented here provide crucial insights into the molecular recognition of the two cofactors, $F_{420}$ and NAD(P)H by FNO.

## Introduction

Flavins can arguably be regarded as the most extensively studied redox cofactors. One natural flavin analogue is cofactor $F_{420}$ which was first isolated and characterized from methanogenic archaea in 1972 (1). Since then, $F_{420}$ has been found in members of methanogens, actinomycetes, cyanobacteria, and some betaproteobacteria (2). Replacement of the 5′ nitrogen of flavins with a carbon in $F_{420}$, resulting in a so-called deazaflavin, renders the cofactor nearly unreactive towards molecular oxygen. Hence, $F_{420}$ is an obligate hydride-transfer cofactor similar to the nicotinamide cofactors (Fig. 1). Besides, the 8′-OH group on the isoalloxazine ring in

$F_{420}$ has been suggested to slow down the autooxidation of the reduced cofactor ($F_{420}H_2$) in air, thus the reduced species is much more stable than that of flavins (3).

Many $F_{420}(H_2)$-dependent enzymes have been characterized recently and their potential for applications in biocatalysis has attracted increasing attention (4,5). $F_{420}$-dependent enzymes studied so far have been shown to be capable of reducing a wide range of substrates which are otherwise recalcitrant to enzyme-catalyzed reduction (4,5). However, the commercial unavailability of cofactor $F_{420}$ remains a bottleneck for studying and applying the respective enzymes. Therefore, it would be attractive to have access to an efficient $F_{420}H_2$ cofactor recycling system. In this context, $F_{420}$:NADPH oxidoreductases (FNOs, E.C. 1.5.1.40, Fig. 1) could become very valuable as NADPH-driven $F_{420}H_2$-recycling systems. FNOs catalyze the reduction of $NADP^+$ using $F_{420}H_2$ and have been found in a number of archaea (6–10) and bacteria (11) (Fig. 1). It has been argued that in methanogens, FNO catalyzes mainly the reduction of $NADP^+$ using $F_{420}H_2$ while bacterial FNOs are supposed to catalyze the reverse reaction (11).

*Thermobifida fusca* is a moderately thermophilic soil bacterium with high G+C content. This actinomycete holds high biocatalytic potential as it has already served as a source for several highly thermostable enzymes, e.g., catalase, Baeyer–Villiger monooxygenase, and glycoside hydrolases (12–14). Interestingly, a recent bioinformatic study predicted that the *T. fusca* genome contains 16 genes encoding for $F_{420}$-dependent enzymes (15). Nevertheless, there has been so far no biochemical evidence for such enzymes. Here, we describe the identification and characterization of a dimeric thermostable $F_{420}$:NADPH oxidoreductase from *T. fusca* (Tfu-FNO), confirming the presence of $F_{420}$-dependent enzymes in this mesophilic bacterium. Despite the high GC content (67%) of the gene sequence, Tfu-FNO is readily expressed in *E. coli*. Notably, Tfu-FNO is a thermostable enzyme and shows a clear substrate preference towards NADP(H) instead of NAD(H). By solving the three-dimensional crystal structure of Tfu-FNO, we set out site-directed mutagenesis to corroborate the role of residues that interact with the phosphate moiety at 2′ position of $NADP^+$.

## Results

### *Purification of Tfu-FNO*

A BLAST search for Af-FNO homologs in *T. fusca* resulted in the identification of the Tfu_0907 gene (TFU_RS04835). The encoded protein shares 40% and 70% sequence identity to FNOs from *A. fulgidus* and *S. griseus*, respectively (Fig. 2). The Tfu-*fno* gene, with a high GC content (67%), was amplified from the genomic DNA of *T. fusca* and transformed into *E. coli* TOP10 as a pBAD-*fno* construct. Purification of the respective protein, Tfu-FNO, was achieved through ammonium sulfate precipitation followed by anion exchange chromatography. DNase I treatment during the first steps of protein purification was found to be essential to remove residual DNA. Tfu-FNO was obtained in pure form with a relatively high yield: 120–200 mg/L culture. It is worth noting that the amount of purified Tfu-FNO obtained in our system is significantly higher than that of Af-FNO when heterologously expressed in *E. coli* [2 mg/L culture (16)].

### *Effects of pH and temperature on activity*

FNOs are known to catalyze the reduction of $NADP^+$ at higher pH, while at lower pH it catalyzes the reverse reaction. Figure 3 shows the effect of pH on Tfu-FNO activity. The reduction rate of $NADP^+$ is highest at pH 8.5–9.0 while the reverse reaction is optimal between pH 4.0–6.0. From the $k_{obs}$ values of both the forward and backward reactions, it can be concluded that FNO catalyzes $NADP^+$ reduction more efficiently (Fig. 3). This is in line with the redox potential of $F_{420}$ (−340 mV) being lower when compared with that of $NADP^+$ (−320 mV) (3).

Since FNO originates from the mesophilic organism *T. fusca*, the enzyme is expected to be stable at relatively high temperatures. Measuring the activities at temperatures between 25 and 90 °C revealed that the enzyme displays highest activity between 60–70 °C (Fig. 4). The activity at 65 °C is almost 4-time higher than that at 25 °C. The apparent melting temperature of Tfu-FNO was found to be 75 °C, as measured by the Thermofluor® method (17). All the generated Tfu-FNO mutants had melting temperatures similar to the wild-type enzyme (data not shown). This indicates that FNO is remarkably thermostable and is most active at elevated temperatures.

*Steady-state kinetics*

The steady-state kinetic parameters were measured for NADPH and $F_{420}$ as substrates by following absorbance of these two cofactors at either 340 nm or 400 nm, respectively. The concentration of one substrate was varied while keeping the other substrate at a constant, saturated concentration. The kinetic data fitted well to the Michaelis–Menten kinetic model when the observed rates ($k_{obs}$) were plotted against substrate concentrations. Tfu-FNO has a $K_m$ value of 7.3 μM and 2.0 μM for NADPH and $F_{420}$, respectively at pH 6.0 and 25 °C (Table 1). Thus, Tfu-FNO has a significantly lower $K_m$ for NADPH (2.0 μM) compared to the values featured by Af-FNO (40 μM) and FNO from *S. griseus* (19.5 μM) (8,11). The $k_{cat}$ (3.3 $s^{-1}$) of Tfu-FNO is somewhat lower when compared with that of Af-FNO (5.27 $s^{-1}$) (18).

*The overall structure of Tfu-FNO*

Crystallization of Tfu-FNO was successful which allowed the elucidation of its crystal structure. This revealed that $NADP^+$ had been co-purified with the native enzyme as it was found to be bound in the active site (Fig. 5–6). All crystal soaking attempts to obtain the $F_{420}$ cofactor bound in the enzyme active site failed, which can be explained by the tight molecular packing found in Tfu-FNO crystals that would hamper cofactor binding in the same position as found in Af-FNO (Fig. 5A). It is known that, depending on the bacterial species, the number of glutamate moieties of $F_{420}$ can vary from two to nine, with five to six being the predominant species in mycobacteria (19). Given the crystal arrangement of Tfu-FNO molecules, an oligoglutamate tail of $F_{420}$ of any length would clash against another subunit interacting through crystal packing (Fig. 5A). Nevertheless, the architecture of the active site is highly conserved, and $NADP^+$ adopts a virtually identical position with respect to that observed in Af-FNO (Fig. 5B). Therefore, $F_{420}$ was tentatively modelled in Tfu-FNO upon superposition of the archaeal enzyme (Fig. 5C). The modelled $F_{420}$ fits very well into the Tfu-FNO active site without any clashes. Similarly to Af-FNO, $F_{420}$ would bind in Tfu-FNO at the C-terminal domain with its deazaisoalloxazine ring burying deep inside the catalytic pocket and the highly polar oligoglutamyl tail directed towards the exterior of the dimer (Fig. 5B,C).

As mentioned above, $NADP^+$ binds to the N-terminal part of Tfu-FNO in a highly similar manner to that of Af-FNO which is characteristic for members of the dinucleotide binding protein family (20,21). The hydrogen bonding network between $NADP^+$ and the residues that form the active site are illustrated in Fig. 6. In particular, the nicotinamide ring directly docks to the protein by hydrogen bonding the cofactor amide group to the peptide nitrogen of Ala155 (corresponding to Ala137 in Af-FNO). This conserved interaction is believed to be crucial in conferring the *trans* conformation of the amide group. With this conformation, the pyridine ring of $NADP^+$ is maintained planar which in turn facilitates the hydride transfer between the C4 of the NADP and C5 of $F_{420}$ by shortening the distance of the two atoms (20).

*$NADP^+$ binding site*

The residues involved in binding the ADP moiety are also conserved in Tfu-FNO (Fig. 6). Analogous to Af-FNO, the negatively charged group of the ribose 2′-phosphate interacts with the side chains of Thr28, Ser50, Arg51, and Arg55 (corresponding to Thr9, Ser31, Arg32, and Lys36 in Af-FNO). These residues are highly conserved in other known FNOs (Fig. 2). These residues therefore appear to be crucial for substrate recognition and help to discriminate between $NADP^+$ and $NAD^+$ (20). To get more insights into the role of these residues, they were mutated into amino acids with different charge and/or size, and tested for the cofactor specificity towards the two nicotinamide cofactors. Table 1 shows the kinetic parameters for both NADH and NADPH as substrate. For wild-type Tfu-FNO, the $K_m$ value for NADH (14 mM) is several orders of magnitude higher than that for NADPH (7.3 μM), clearly confirming that the enzyme prefers NADP(H) over NAD(H). For all mutants, the $K_m$ value for NADPH significantly increased (from 2.6- to >68-fold) compared to that of the wild-type enzyme, which verified the crucial role of these residues in binding NADP(H). Intriguingly, recognition of NADH remained the same or improved in all mutants (Table 3), with a $K_m$ value ranging from 0.23- to 2.3-times of that from the wild-type. Noticeably, R55N and R55S variants have a significantly improved affinity towards NADH. In case of mutant R55N, $K_{m,\ NADPH}$ increased more than 100 fold while the $K_{m,\ NADH}$ decreased almost 4 fold. The S50E mutant was the best among the tested mutants with a $K_{m,\ NADH}$ of almost 5-time lower and a $K_{m,}$

$_{NADPH}$ of approximately 100-fold higher as compared to wild-type Tfu-FNO. Interestingly, the T28A mutant showed an increased activity towards both NADPH and NADH, with a 4-fold increase in catalytic rate ($k_{cat}$ = 14 $s^{-1}$) for NADPH and a 2.8-fold decrease in $K_m$ value (5 mM) for NADH when compared with the wild-type enzyme. This resulted in significantly improved $k_{cat}/K_m$ values for both NADPH and NADH, respectively. Unfortunately, combinations of the mutations did not show significant additive effects (Table 1).

## Discussion

$F_{420}$-dependent enzymes are interesting candidates for biotechnological applications (5). Recent studies have suggested a widespread occurrence of such deazaflavin-dependent enzymes in actinobacteria (15). Some specific lineages seem especially rich in $F_{420}$-dependent enzymes, such as *Mycobacterium tuberculosis*. This makes members of this superfamily of deazaflavoproteins potential drug targets due to their absence in the human proteome and the human gut flora. The work of Selengut et al. also predicted the presence of at least 16 $F_{420}$ related genes in *T. fusca,* including all genes required for $F_{420}$ biosynthesis (15). Through our study, we have experimentally confirmed the presence of an $F_{420}$-dependent enzyme in this actinomycete by cloning and characterization of a thermostable $F_{420}$:NADPH oxidoreductase (Tfu-FNO), which catalyzes the reduction of $NADP^+$ using reduced $F_{420}$ and the reverse reaction.

*The role of FNO in generating reduced $F_{420}$*

$F_{420}$ cofactor provides microorganism alternative redox pathways. The deazaflavin cofactor seems especially equipped for reduction reactions as it displays a redox potential which is lower when compared with the nicotinamide cofactor. Two enzymes have been identified in previous studies that serve a role in reducing $F_{420}$—FNO and $F_{420}$-dependent glucose-6-phosphate dehydrogenase (FGD) (4). Using *T. fusca* cell-free extract and heterologously expressed Tfu_1669 (a putative *M. tuberculosis* FGD homolog), we could not detect any FGD activity (unpublished data). This suggests that the *T. fusca* proteome indeed does not include an FGD. In fact, it has been shown before that not all actinomycetes have an FGD (22). Therefore, FNO may be the primary enzyme in actinomycetes for providing the cells with $F_{420}H_2$. Nevertheless, at physiological pH (7.0–8.0, Fig. 3) Tfu-FNO performs reduction of $NADP^+$ slightly better than reduction of cofactor $F_{420,}$ which is different from the FNO from *S. griseus* (11) and more similar to the archaeal FNOs (7,8). This can partly be explained by the experimental condition (24 °C) differing from the optimum temperature at which the bacteria grow (55 °C) and the intercellular environment (e.g., cofactor concentrations, salt concentrations). Several lines of evidence suggest that in other actinomycetes, such as *Rhodococcus opacus* and *Nocardioides simplex*, FNO is also the main source of $F_{420}H_2$. In these bacteria, the *fno* gene was embedded in the same operon with genes encoding for the $F_{420}H_2$-dependent reductases, which are involved in the metabolism of picrate and 2,4-dinitrophenols (23–25). FNO-catalyzed regeneration of $F_{420}H_2$ was also proposed to be crucial for the reductive steps in the biosynthesis of tetracycline by *Streptomyces* (26).

*Structure and NADP(H) binding site of Tfu-FNO*

FNO is believed to be the only $F_{420}$-dependent enzyme known so far that is conserved between archaea and bacteria (4). Except for a 19 amino acid extension loop at the N-terminus, Tfu-FNO largely shares the overall topology and cofactor binding site with that from *A. fulgidus* (Fig. 2 and 5B). The residues that interact directly with the 2′-phosphate group of NADP(H) are also highly conserved (Fig. 6), and have proven to be essential for binding this cofactor. Upon disrupting the hydrogen bonding network by mutagenesis, all the mutants lost virtually all ability to recognize NADPH (Table 1). Intriguingly, the affinity of these variants towards NADH improved, with the T28A mutant being the best in terms of specificity for NADH (3.3-fold higher $k_{cat}/K_m$ than that of WT). Yet, an efficient NADH-dependent FNO has still to be engineered. For this, a newly developed tool could be explored which can guide structure-inspired switching of coenzyme specificity (27).

*Potential applications in biocatalysis*

Tfu-FNO represents a highly attractive candidate for the biocatalytic reduction of $F_{420}$. The enzyme is very thermostable, remains active over a wide range of pH (Fig. 3,4), and can be easily expressed in *E. coli* (120–200 mg/ L culture). Tfu-FNO is also a relatively fast enzyme, especially with the T28A mutant displaying a $k_{cat}$ of 14 $s^{-1}$ for NADPH (Table 1). Whereas the majority of current enzymatic $F_{420}H_2$ regeneration protocols employ FGDs (28,29), the cost of the expensive, non-recyclable cosubstrate glucose-6-phosphate remains the main bottleneck for the use of such enzyme in large-scale

applications. Therefore, an $F_{420}H_2$-generating system whose cosubstrate could be recycled, such as T28A TfuFNO would be highly promising. Available, robust NAD(P)H regeneration machineries, such as glucose dehydrogenase or other dehydrogenases, have been thoroughly investigated and widely applied in industry (30). Therefore, by combining Tfu-FNO with an appropriate NAD(P)H recycler, $F_{420}H_2$-reductases can be exploited for biocatalytic purposes.

## Experimental procedures

*Cloning, expression, and purification of Tfu-FNO*

*Thermobifida fusca* YX was grown at 55 °C in Hägerdahl medium and its genomic DNA was extracted using the GeneElute Bacterial Genomic DNA kit (Sigma–Aldrich). The gene Tfu-*fno* (Tfu_0970, TFU_RS04835) was PCR amplified from genomic DNA of *T. fusca* using the pair of primers listed in Table 2 with the *Nde*I and *Hind*III restriction sites introduced at the 5′ and 3′ positions of the gene, respectively. The purified PCR product and the pBAD*N*/*Myc*-HisA vector were digested with the restriction enzymes *Nde*I and *Hind*III, purified, and ligated [vector to insert ratio ca. 1 to 5 (mol/mol)] using T4 DNA ligase (Promega) with quick ligation buffer. The pBAD*N*/*Myc*-HisA vector is a variant of the commercial pBAD/*Myc*-HisA (Invitrogen) where the unique *Nco*I site at the translation start is replaced with *Nde*I. The ligation product was transformed into chemically competent *E. coli* TOP10 cells using the heat shock method. Correct transformants were confirmed by sequencing the recombinant plasmid pBAD-*fno*.

Site-directed mutagenesis was carried out by using the pBAD-*fno* vector as template and the QuikChange® mutagenesis method with the corresponding pairs of primers listed in Table 2. The primers (200 nM) were used in a 10 µL reaction mixture. In case of the double mutants, plasmids with a single mutation were used as template. The remaining parent template vector was digested by incubating with *Dpn*I (New England Biolab) at 37 °C for 2 h. *Dpn*I was then inactivated at 80 °C for 10 min and the mutant plasmid was transformed into chemically competent *E. coli* TOP10 cells. Mutations were confirmed by sequencing.

*E. coli* TOP10 cells with pBAD-*fno* were grown overnight at 37 °C, 130 rpm in a 5 ml lysogenic broth (LB) containing 50 µg/ml ampicillin. This pre-culture was used to inoculate 500 ml of the same medium and grown at 37 °C, 130 rpm. When the $OD_{600}$ reached 0.4–0.6, the protein expression was induced by addition of 0.02% (w/v) arabinose followed by incubation at 30 °C, 130 rpm for 12 h. Cells were harvested by centrifugation at 6000 × g for 15 min (JLA 10.500 rotor, 4 °C) and resuspended in 10 ml of 50 mM KPi pH 7.0 supplemented with 1 µg/ml of DNase I. Cells were sonicated for 7 min (10 sec on, 15 sec off cycle, 70% amplitude) at 4 °C using a VCX130 Vibra-Cell sonicator (Sonics & Materials, Inc., Newton, USA), and then centrifuged at 15000 × g (JA 17 rotor) for 45 min to obtain the cell-free extract. Tfu-FNO was precipitated by adding 50% saturated ammonium sulfate followed by anion exchange chromatography with a HiTrap™ Q HP 5ml (GE Healthcare) column pre-equilibrated with the same resuspension buffer. Tfu-FNO was eluted by using a linear gradient of 0–1 M NaCl in the same buffer. At around 250 mM NaCl, Tfu-FNO started eluting. Excess salt was removed by using PD-10 desalting column and the protein was stored in 50 mM KPi buffer. (GE Healthcare). Protein concentration was estimated using Bradford assay (30).

*Temperature, pH optima, and thermostability of Tfu-FNO*

$F_{420}$ was isolated from *Mycobacterium smegmatis* $mc^2$ 4517 as previously published protocol (32). $F_{420}H_2$ was prepared by biocatalytic reduction of $F_{420}$ using a recombinant $F_{420}$-dependent glucose-6-phosphate dehydrogenase from *Rhodococcus jostii* RHA1 (29) as previously described (28).

The apparent melting temperature, $T_m$, was determined using the *Thermoflour*® technique (17) with a Bio-Rad C1000 Touch Thermal Cycler (Bio-rad Laboratories, Inc.). The reaction volume was 25 µL, containing 10 µM of enzyme and 5 µL of 5 × SYPRO Orange (Invitrogen). To determine the temperature for optimal activity of Tfu-FNO, the enzyme activity was measured using 1.25 mM NADPH and 20 µM $F_{420}$ in 50 mM KPi pH 6.0 in a 100 µL reaction volume. The cuvette containing the substrates in preheated buffer was heated to the tested temperature (25–90 °C) and the reaction was started by adding 10 nM enzyme. The pH optimum was determined for both the forward and backward reactions of Tfu-FNO. $F_{420}$ depletion at 400 nm ($\varepsilon_{400}$ = 25 $mM^{-1}$ $cm^{-1}$) (33,34) or NADH formation at 340 nm ($\varepsilon_{340}$ = 6.22 $mM^{-1}$ $cm^{-1}$) was followed using a V-660 spectrophotometer from Jasco (IJsselstein, The Netherlands). In this experiment, the reaction (100 µL) contained 250 µM NADPH and 20 µM $F_{420}$ ($F_{420}$ reduction); or 250 µM $NADP^+$ and 20 µM

$F_{420}H_2$ ($NADP^+$reduction) in 50 mM buffer. Sodium acetate, KPi and Tricine-KOH based buffers were used for pH 4.5–5.5, 6.0–7.5 and 8.0–9.5, respectively.

*Steady-state kinetic analyses*

To determine the kinetic parameters of the enzyme, initial $F_{420}$ reduction rates were measured using a SynergyMX microplate reader (BioTek) using 96-well F-bottom plates (Greiner Bio-One GmbH) at 25 °C. The reaction was performed in 50 mM KPi pH 6.0 and was started by adding 25–50 nM enzyme in the final volume of 200 µL. The concentration of one of the substrates was kept constant (250 µM for NADPH and 20 µM for $F_{420}$, respectively) while varying the concentration of the other substrate. All the measurements were performed in duplicate. A decrease of absorption either at 400 nm ($F_{420}$ reduction, $\varepsilon_{400}$ = 25.7 $mmol^{-1}$ $cm^{-1}$) or at 340 nm (NADPH oxidation, $\varepsilon_{340}$ = 6.22 $mmol^{-1}$ $cm^{-1}$) was followed to determine the observed rates, $k_{obs}$ ($s^{-1}$). $K_m$ and $k_{cat}$ values for $NADP^+$, NADPH, $F_{420}$ and $F_{420}H_2$ were calculated by fitting the data into the Michaelis–Menten kinetic model using nonlinear regression with GraphPad Prism 6.00 (GraphPad Software, La Jolla, CA, USA).

*Crystallization, X-ray data collection, and structure determination of Tfu-FNO*

Native Tfu-FNO was crystallized using the sitting-drop vapour diffusion technique at 20 °C by mixing equal volumes of 9.0 mg/mL protein in 10 mM Tris/HCl pH 7.5, 100 mM NaCl and of the reservoir solution containing 5% (w/v) PEG 3000, 30% (v/v) PEG 400, 10% (v/v) glycerol, 0.1 M HEPES pH 7.5. Prior to data collection, crystals were cryo-protected in the mother liquor and flash-cooled by plunging them into liquid nitrogen. X-ray diffraction data to 1.8 Å were collected at the ID30B beamline of the European Synchrotron Radiation Facility in Grenoble, France (ESRF). Image indexing, integration, and data scaling were processed with XDS package (35,36) and programs of the CCP4 suite (37). The Tfu-FNO structure was initially solved by molecular replacement method with Phaser (38) using the coordinates of FNO from *A. fulgidus* [PDB ID code 1JAY (20)] which shares 40% sequence identity with Tfu-FNO as a starting model devoid of all ligands and water molecules. Manual model correction and structure analysis was carried out with Coot (39) whereas alternating cycles of refinement was performed with Refmac5 (40). Figures were generated by using UCSF Chimera (41). Atomic coordinates and structure factors were deposited in the Protein Data Bank under the accession code 5N2I. Detailed data processing and refinement statistics are available in Table 3.

## Acknowledgements

This work was supported by an Erasmus Mundus action 2 “Svaagata” program from the European Commission via a PhD scholarship provided to HK and a Ubbo Emmius scholarship from the University of Groningen, the Netherlands, awarded to QTN. We thank the European Synchrotron Radiation Facility (ESRF) for providing beamtime and assistance. We are grateful to Dr. G. Bashiri at the Structural Biology Laboratory, School of Biological Sciences and Maurice Wilkins Centre for Molecular Biodiscovery, the University of Auckland, New Zealand for generously providing a culture of *M. smegmatis* $mc^2$ 4517 and the plasmid pYUBDuet-FbiABC. A. Giusti, S. Rovida and F. Forneris are acknowledged for their experimental support.

## Conflict of interest

The authors declare that they have no conflicts of interest with the contents of this article.

## Author contributions

HK and MWF conceived the study and designed the experiments. HK performed the cloning, expression, purification, and biochemical characterization of the Tfu-FNO wild-type and variants. QTN performed the crystallization and solved the structure of Tfu-FNO. AM and CB supervised this part of the study. HK and QTN drafted the manuscript. All authors contributed to analyzing the data and writing the paper.

## References

1. Cheeseman, P., Toms–Wood, A., and Wolfe, R.S. (1972) Isolation and properties of a fluorescent compound, factor 420, from *Methanobacterium* strain M.o.H. *J. Bacteriol.* **112,** 527–531

2. Daniels, L., Bakhiet, N., and Harmon, K. (1985) Widespread distribution of a 5-deazaflavin cofactor in *Actinomyces* and related bacteria. *Syst. Appl. Microbiol.* **6,** 12–17

3. Jacobson, F., and Walsh, C. (1984) Properties of 7,8-didemethyl-8-hydroxy-5-deazaflavins relevant to redox coenzyme function in methanogen metabolism. *Biochemistry (N.Y.)* **23,** 979–988

4. Greening, C., Ahmed, F.H., Mohamed, A.E., Lee, B.M., Pandey, G., Warden, A.C., Scott, C., Oakeshott, J.G., Taylor, M.C., and Jackson, C.J. (2016) Physiology, biochemistry, and applications of $F_{420}$- and $F_o$-dependent redox reactions. *Microbiol. Mol. Biol. Rev.* **80,** 451–493

5. Taylor, M., Scott, C., and Grogan, G. (2013) $F_{420}$-dependent enzymes—potential for applications in biotechnology. *Trends Biotechnol.* **31,** 63–64

6. Eirich, L.D., and Dugger, R.S. (1984) Purification and properties of an $F_{420}$-dependent NADP reductase from *Methanobacterium thermoautotrophicum. Biochim. Biophys. Acta (BBA)–General Subjects.* **802,** 454–458

7. de Wit, L., and Eker, A. (1987) 8-Hydroxy-5-deazaflavin-dependent electron transfer in the extreme halophile *Halobacterium cutirubrum. FEMS Microbiol. Lett.* **48,** 121–125

8. Kunow, J., Schwörer, B., Stetter, K.O., and Thauer, R.K. (1993) A $F_{420}$-dependent NADP reductase in the extremely thermophilic sulfate-reducing *Archaeoglobus fulgidus*. *Arch. Microbiol.* **160,** 199–205

9. Berk, H., and Thauer, R.K. (1997) Function of coenzyme $F_{420}$-dependent NADP reductase in methanogenic archaea containing an NADP-dependent alcohol dehydrogenase. *Arch. Microbiol.* **168,** 396–402

10. Elias, D.A., Juck, D.F., Berry, K.A., and Sparling, R. (2000) Purification of the $NADP^+$:$F_{420}$ oxidoreductase of *Methanosphaera stadtmanae*. *Can. J. Microbiol.* **46,** 998–1003

11. Eker, A., Hessels, J., and Meerwaldt, R. (1989) Characterization of an 8-hydroxy-5-deazaflavin: NADPH oxidoreductase from *Streptomyces griseus*. *Biochim. Biophys. Acta (BBA)–General Subjects.* **990,** 80–86

12. Wilson, D.B. (2004) Studies of *Thermobifida fusca* plant cell wall degrading enzymes. *Chem. Rec.* **4,** 72–82

13. Fraaije, M.W., Wu, J., Heuts, D.P., van Hellemond, E.W., Spelberg, J.H.L., and Janssen, D.B. (2005) Discovery of a thermostable Baeyer–Villiger monooxygenase by genome mining. *Appl. Microbiol. Biotechnol.* **66,** 393–400

14. Lončar, N., and Fraaije, M.W. (2015) Not so monofunctional—a case of thermostable *Thermobifida fusca* catalase with peroxidase activity. *Appl. Microbiol. Biotechnol*. **99,** 2225–2232

15. Selengut, J.D., and Haft, D.H. (2010) Unexpected abundance of coenzyme $F_{420}$-dependent enzymes in *Mycobacterium tuberculosis* and other actinobacteria. *J. Bacteriol.* **192,** 5788–5798

16. Le, C.Q., Joseph, E., Nguyen, T., and Johnson-Winters, K. (2015) Optimization of expression and purification of recombinant *Archeoglobus fulgidus* $F_{420}H_2$:$NADP^+$ oxidoreductase, an $F_{420}$ cofactor dependent enzyme. *Protein J.* **34,** 391–397

17. Pantoliano, M.W., Petrella, E.C., Kwasnoski, J.D., Lobanov, V.S., Myslik, J., Graf, E., Carver, T., Asel, E., Springer, B.A., Lane, P., and Salemme, F.R. (2001) High–density miniaturized thermal shift assays as a general strategy for drug discovery. *J. Biomol. Screen.* **6,** 429–440

18. Hossain, M.S., Le, C.Q., Joseph, E., Nguyen, T.Q., Johnson–Winters, K., and Foss, F.W. (2015) Convenient synthesis of deazaflavin cofactor FO and its activity in $F_{420}$-dependent NADP reductase. *Org. Biomol. Chem.* **13,** 5082–5085

19. Bair, T.B., Isabelle, D.W., and Daniels, L. (2001) Structures of coenzyme $F_{420}$ in *Mycobacterium* species. *Arch. Microbiol.* **176,** 37–43

20. Warkentin, E., Mamat, B., Sordel–Klippert, M., Wicke, M., Thauer, R.K., Iwata, M., Iwata, S., Ermler, U., and Shima, S. (2001) Structures of $F_{420}H_2$:$NADP^+$ oxidoreductase with and without its substrates bound. *EMBO J.* **20,** 6561–6569

21. Carugo, O., and Argos, P. (1997) NADP-dependent enzymes. II: Evolution of the mono-and dinucleotide binding domains. Proteins: *Struct. Funct. Genet.* **28,** 29–40

22. Purwantini, E., Gillis, T.P., and Daniels, L. (1997) Presence of $F_{420}$-dependent glucose-6-phosphate dehydrogenase in *Mycobacterium* and *Nocardia* species, but absence from *Streptomyces* and *Corynebacterium* species and methanogenic archaea. *FEMS Microbiol. Lett.* **146,** 129–134

23. Heiss, G., Hofmann, K.W., Trachtmann, N., Walters, D.M., Rouvière, P., and Knackmuss, H. (2002) *npd* gene functions of *Rhodococcus* (*opacus*) *erythropolis* HL PM-1 in the initial steps of 2,4,6-trinitrophenol degradation. *Microbiology.* **148,** 799–806

24. Ebert, S., Fischer, P., and Knackmuss, H. (2001) Converging catabolism of 2,4,6-trinitrophenol (picric acid) and 2,4-dinitrophenol by *Nocardioides simplex* FJ2-1A. *Biodegradation.* **12,** 367–376

25. Ebert, S., Rieger, P.G., and Knackmuss, H.J. (1999) Function of coenzyme $F_{420}$ in aerobic catabolism of 2,4,6-trinitrophenol and 2,4-dinitrophenol by *Nocardioides simplex* FJ2–1A. *J. Bacteriol.* **181,** 2669–2674

26. Novotná, J., Neužil, J., and Hošťálek, Z. (1989) Spectrophotometric identification of 8-hydroxy-5-deazaflavin:NADPH oxidoreductase activity in streptomycetes producing tetracyclines. *FEMS Microbiol. Lett.* **59,** 241–245

27. Cahn, J.K., Werlang, C.A., Baumschlager, A., Brinkmann-Chen, S., Mayo, S.L., and Arnold, F.H. (2017) A General Tool for Engineering the NAD/NADP Cofactor Preference of Oxidoreductases. *ACS Synth. Biol.* **6,** 326–333

28. Manjunatha, U.H., Boshoff, H., Dowd, C.S., Zhang, L., Albert, T.J., Norton, J.E., Daniels, L., Dick, T., Pang, S.S., and Barry, C.E.,3rd (2006) Identification of a nitroimidazo-oxazine-specific protein involved in PA-824 resistance in *Mycobacterium tuberculosis*. *Proc. Natl. Acad. Sci. U.S.A.* **103,** 431–436

29. Nguyen, Q.-T., Trinco, G., Binda, C., Mattevi, A., and Fraaije, M.W. (2016) Discovery and characterization of an $F_{420}$-dependent glucose-6-phosphate dehydrogenase (Rh-FGD1) from *Rhodococcus jostii* RHA1. *Appl. Microbiol. Biotechnol*. 10.1007/s00253-016-8038-y

30. Wichmann, R., and Vasic–Racki, D. (2005) Cofactor regeneration at the lab scale. *Adv. Biochem. Eng. Biotechnol.* **92,** 225–260

31. Bradford, M.M. (1976) A rapid and sensitive method for the quantitation of microgram quantities of protein utilizing the principle of protein–dye binding. *Anal. Biochem.* **72,** 248–254

32. Isabelle, D., Simpson, D.R., and Daniels, L. (2002) Large-scale production of coenzyme $F_{420}$-5,6 by using *Mycobacterium smegmatis*. *Appl. Environ. Microbiol.* **68,** 5750–5755

33. Jacobson, F.S., Daniels, L., Fox, J.A., Walsh, C.T., and Orme–Johnson, W.H. (1982) Purification and properties of an 8-hydroxy-5-deazaflavin-reducing hydrogenase from *Methanobacterium thermoautotrophicum*. *J. Biol. Chem.* **257,** 3385–3388

34. DiMarco, A.A., Bobik, T.A., and Wolfe, R.S. (1990) Unusual coenzymes of methanogenesis. *Annu. Rev. Biochem.* **59,** 355–394

35. Kabsch, W. (2010) Xds. *Acta Crystallographica Section D: Biological Crystallography.* **66,** 125–132

36. Kabsch, W. (2010) Integration, scaling, space-group assignment and post-refinement. *Acta. Crystallogr. Sect. D: Biol. Crystallogr.* **66,** 133–144

37. Winn, M.D., Ballard, C.C., Cowtan, K.D., Dodson, E.J., Emsley, P., Evans, P.R., Keegan, R.M., Krissinel, E.B., Leslie, A.G., McCoy, A., McNicholas, S.J., Murshudov, G.N., Pannu, N.S., Potterton, E.A., Powell, H.R., Read, R.J., Vagin, A., and Wilson, K.S. (2011) Overview of the CCP4 suite and current developments. *Acta Crystallogr. Sect. D: Biol. Crystallogr.* **67,** 235–242

38. McCoy, A.J., Grosse-Kunstleve, R.W., Adams, P.D., Winn, M.D., Storoni, L.C., and Read, R.J. (2007) Phaser crystallographic software. *J. Appl. Crystallogr.* **40,** 658–674

39. Emsley, P., and Cowtan, K. (2004) Coot: model-building tools for molecular graphics. *Acta Crystallogr. Sect. D: Biol.Crystallogr.* **60,** 2126–2132

40. Murshudov, G.N., Vagin, A.A., and Dodson, E.J. (1997) Refinement of macromolecular structures by the maximum–likelihood method. *Acta Crystallogr. Sect. D: Biol.Crystallogr.* **53,** 240–255

41. Pettersen, E.F., Goddard, T.D., Huang, C.C., Couch, G.S., Greenblatt, D.M., Meng, E.C., and Ferrin, T.E. (2004) UCSF Chimera—a visualization system for exploratory research and analysis. *J. Comput. Chem.* **25,** 1605–1612

**Table 1** Steady-state kinetic parameters for wild-type and mutant Tfu-FNOs using NADH and NADPH as substrate. n.d., not determined.

| Tfu-FNO variant | NADH | | | NADPH | | | $k_{cat}/K_{m,\ NADPH}/k_{cat}/K_{m,\ NADH}$ |
|---|---|---|---|---|---|---|---|
| | $K_m$ (mM) | $k_{cat}$ ($s^{-1}$) | $k_{cat}/K_m$ ($M^{-1}\ s^{-1}$) | $K_m$ (μM) | $k_{cat}$ ($s^{-1}$) | $k_{cat}/K_m$ ($mM^{-1}\ s^{-1}$) | |
| Wild-type | 14 ± 4.2 | 2.2 ± 0.4 | 160 | 7.3 ± 1.0 | 3.3 ± 0.1 | 450 | 2800 |
| R51A | 8.6 ± 0.9 | 3.2 ± 0.2 | 370 | >180 | >1.6 | 6.2 | 17 |
| R51V | 8.7 ± 1.1 | 3.4 ± 0.2 | 290 | >180 | >1.3 | 9.3 | 32 |
| R55A | 7.0 ± 0.8 | 3.0 ± 0.2 | 420 | 29 ± 4.0 | 8.8 ± 0.3 | 300 | 710 |
| R55N | 6.3 ± 3.6 | 2.8 ± 0.7 | 440 | >500 | n.d. | | |
| R55S | 4.4 ± 1.3 | 3.5 ± 0.4 | 790 | 170 ± 38 | 6.9 ± 0.7 | 41 | 52 |
| R55V | 9.6 ± 1.4 | 3.2 ± 0.2 | 330 | 49 ± 7.2 | n.d. | | |
| S50E | 3.2 ± 1.0 | 2.7 ± 0.3 | 840 | >500 | n.d. | | |
| S50Q | 8.2 ± 2.7 | 4.2 ± 0.6 | 510 | >500 | n.d. | | |
| T28A | 5.0 ± 0.6 | 2.6 ± 0.1 | 520 | 19 ± 2.6 | 14 ± 0.5 | 720 | 1400 |
| R51ER55A | 10 ± 2.7 | 1.6 ± 0.2 | 160 | >500 | n.d. | | |
| R51ER55N | 6.5 ± 1.3 | 2.7 ± 0.2 | 420 | >500 | n.d. | | |
| R51ER55S | 32 ± 1.9 | 4.9 ± 0.2 | 150 | >500 | n.d. | | |
| R51VR55V | 10 ± 1.4 | 2.8 ± 0.2 | 280 | >500 | n.d. | | |
| S50ER55A | 20 ± 9.2 | 2.3 ± 0.7 | 120 | >500 | n.d. | | |
| S50ER55V | 9.8 ± 2.3 | 1.8 ± 0.2 | 180 | >500 | n.d. | | |
| T28AR51V | 12 ± 2.2 | 2.7 ± 0.3 | 230 | >500 | n.d. | | |
| T28AR55A | 5.4 ± 1.5 | 2.5 ± 0.3 | 460 | 93 ± 29 | 3.3 ± 0.4 | 3.5 | 8 |
| T28AR51VR55V | 12 ± 2.2 | 3.3 ± 0.3 | 280 | >500 | n.d. | | |

**Table 2** Primers used in this study. Sites of mutations are marked with oligonucleotides in bold, whereas restriction sites are in bold, italic.

| *fno* genes | Forward primers (5′–3′) | Reverse primers (5′–3′) |
|---|---|---|
| FNO WT | TGC***CATATG***TCGATTGCCGTGCTG TCG | ***AAGCTT***TAGATGTCGGTGATGCGGATAC |
| FNO_R51M | TGATTCTCGGTTCG**ATG**AGCGCGGAGCGGG | CCCGCTCCGCGCT**CAT**CGAACCGAGAATCA |
| FNO_S50Q | GCACGAGGTGATTCTCGGT**CAG**CGGAGCGCG | CGCGCTCCG**CTG**ACCGAGAATCACCTCGTGC |
| FNO_S50E | GCACGAGGTGATTCTCGGT**GAG**CGGAGCGCG | CGCGCTCCG**CTC**ACCGAGAATCACCTCGTGC |
| FNO_R55S | GGAGCGCGGAG**AGC**GCCCAGGCGGT | ACCGCCTGGGC**GCT**CTCCGCGCTCC |
| FNO_R55N | GCGGAGCGCGGAG**AAC**GCCCAGGCGGTTG | CAACCGCCTGGGC**GTT**CTCCGCGCTCCGC |
| FNO_T28A | GTGCTGGGGGGC**GCG**GGTGATCAGG | CCTGATCACC**CGC**GCCCCCCAGCAC |
| FNO_R51A | GATTCTCGGTTCG**GCG**AGCGCGGAGCGG | CCGCTCCGCGCT**CGC**CGAACCGAGAATC |
| FNO_R51V | GATTCTCGGTTCG**GTG**AGCGCGGAGCGG | CCGCTCCGCGCT**CAC**CGAACCGAGAATC |
| FNO_R51E | GATTCTCGGTTCG**GAG**AGCGCGGAGCGG | CCGCTCCGCGCT**CTC**CGAACCGAGAATC |
| FNO_R55A | GGAGCGCGGAG**GCG**GCCCAGGCGG | CCGCCTGGGC**CGC**CTCCGCGCTCC |
| FNO_R55V | GGAGCGCGGAG**GTG**GCCCAGGCGG | CCGCCTGGGC**CAC**CTCCGCGCTCC |
| FNO_R55E | GGAGCGCGGAG**GAG**GCCCAGGCGG | CCGCCTGGGC**CTC**CTCCGCGCTCC |
| FNO_S50A | ACGAGGTGATTCTCGGT**GCG**CGGAGCG | CGCTCCG**CGC**ACCGAGAATCACCTCGT |

**Table 3** Data collection and refinement statistics

| | |
|---|---|
| PDB ID Code | 5N2I |
| Space group | $P2_12_12_1$ |
| Resolution (Å) | 1.80 |
| *a*, *b*, *c* (Å) | 82.4, 86.1,136.8 |
| $R_{sym}$[a,b] (%) | 11.2 (99.1) |
| Completeness[b] (%) | 98.6 (90.2) |
| Unique reflections | 89383 |
| Multiplicity[b] | 4.5 (2.8) |
| I/σ[b] | 7.9 (0.9) |
| $CC_{1/2}$[b] | 99.4 (24.7) |
| Number of atoms: | |
| protein | 6594 |
| $NADP^+$/glycerol/water | 4 × 48/7 × 6/600 |
| Average B value for all atoms ($Å^2$) | 25.0 |
| $R_{cryst}$[b,c] (%) | 16.5 (34.1) |
| $R_{free}$[b,c] (%) | 21.4 (35.7) |
| Rms bond length (Å) | 0.019 |
| Rms bond angles (°) | 2.02 |
| Ramachandran outliers | 0 |

[a] $R_{sym} = \sum|I_i - <I>|/\sum I_i$, where $I_i$ is the intensity of $i^{th}$ observation and <I> is the mean intensity of the reflection.
[b] Values in parentheses are for reflections in the highest resolution shell.
[c] $R_{cryst} = \sum|F_{obs} - F_{calc}|/\sum|F_{obs}|$ where $F_{obs}$ and $F_{calc}$ are the observed and calculated structure factor amplitudes, respectively. $R_{cryst}$ and $R_{free}$ were calculated using the working and test sets, respectively.

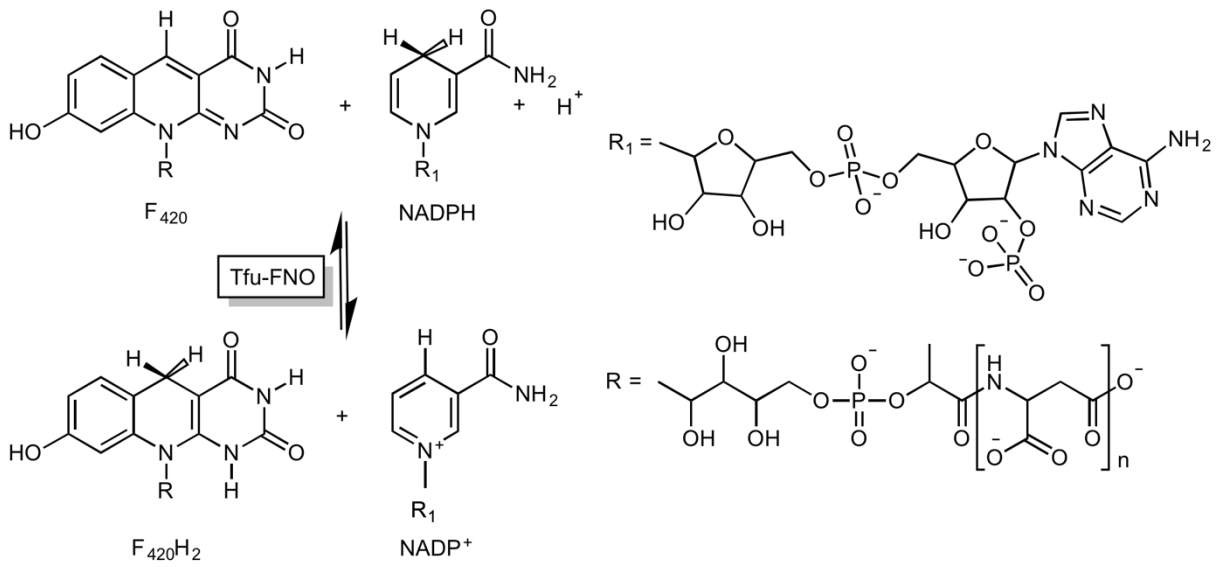


**Figure 1** The reversible reaction catalyzed by $F_{420}$:NADPH oxidoreductase. The number of glutamate residues attached to the phospholactyl moiety may vary (n = 2–8 in case of *Mycobacterium smegmatis*).

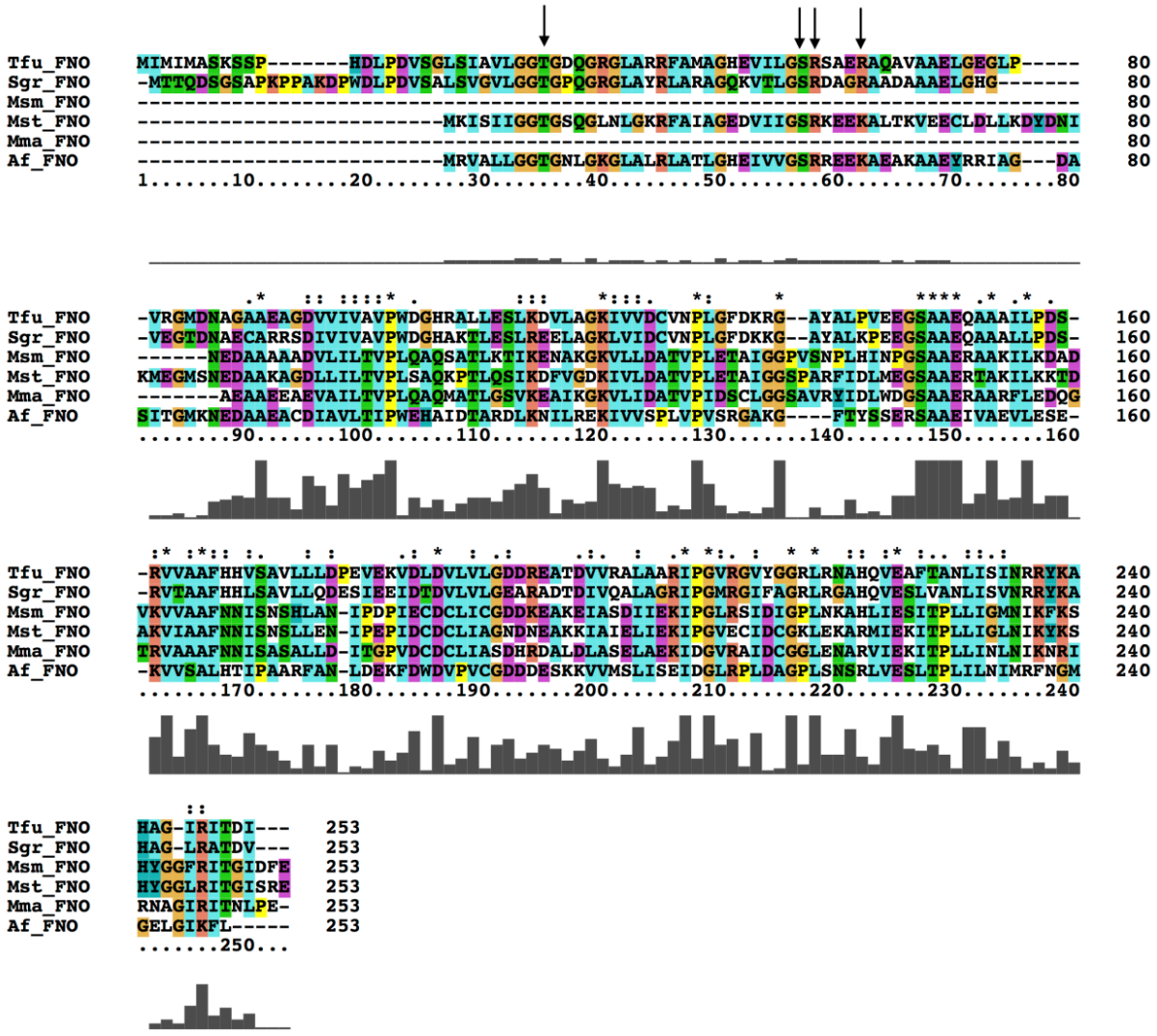


**Figure 2** Multiple sequence alignment of selected FNOs from *Thermobifida fusca* (Tfu_FNO), *Archaeoglobus fulgidus* (Af_FNO), *Methanothermobacter marburgensis* (Mma_FNO), *Methanobrevibacter smithii* (Msm_FNO), *Methanosphaera stadtmanae* (Mst_FNO), and *Streptomyces griseus* (Sgr_FNO). The figure was generated with Clustal X2.1. Residues involved in binding the 2′-phosphate group of $NADP^+$ are indicated with an arrow.

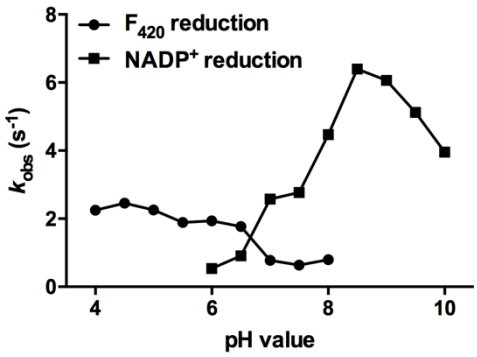


**Figure 3** pH optimum for the Tfu-FNO-catalyzed $F_{420}$ reduction using NADPH (dots) or the $NADP^+$ reduction using $F_{420}H_2$ (squares) at 24 °C. $k_{obs}$ ($s^{-1}$) for the $NADP^+$ reduction (pH optima 8–10) is almost 3-time higher than that for the $F_{420}$ reduction (pH optimum 4–6).

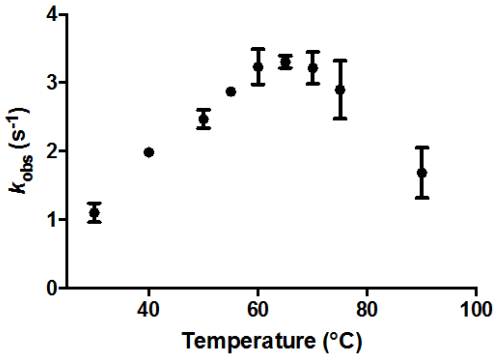


**Figure 4** Effect of temperature on Tfu-FNO activity. Reaction mixture of 100 µL contained 1.25 mM NADH, 20 µM $F_{420}$ in 50 mM KPi pH 6.0. The reaction was started by adding 50 nM FNO. The error bars represent standard deviation from two measurements.

**A**

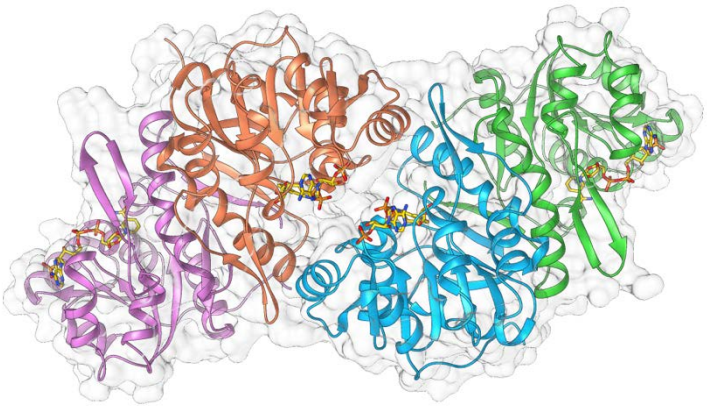

**B**

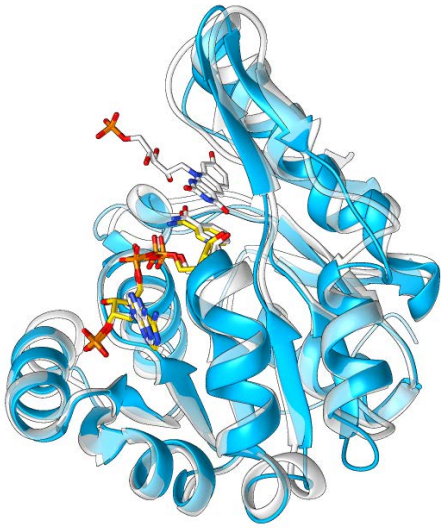

**C**

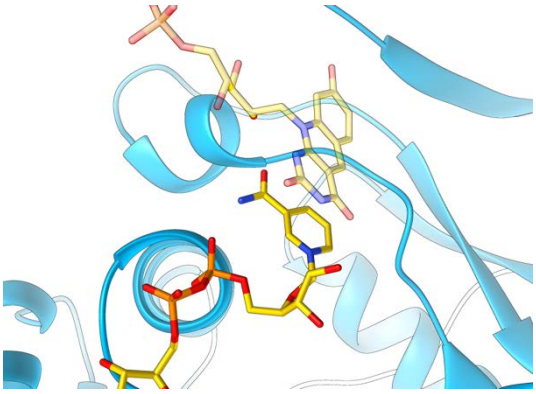

**Figure 5** Crystal structure of FNO from *Thermobifida fusca* (**A)** The asymmetric unit of Tfu-FNO crystals contain two dimers AB and CD, colored in coral (monomer A), orchid (monomer B), deep sky blue (monomer C), and green (monomer D), respectively. (**B**) Superposition of the Tfu-FNO monomer C onto the homologous $NADP^+$- and $F_{420}$-bound Af-FNO monomer [carbon atoms in white, 40% sequence identity, PDB ID 1JAY (20)]. The two structures largely share the same overall topology and the binding pocket architecture, with the nicotinamide rings adopting a similar position in the active site. (**C**) Close-up view of Tfu-FNO binding pocket with a modelled $F_{420}$ molecule (in

shaded colors with carbon atoms in yellow) as a result of superposition as in **B**. The NADP(H) carbon atoms are shown in yellow, oxygen atoms in red, nitrogen atoms in blue, and phosphorous atoms in orange.

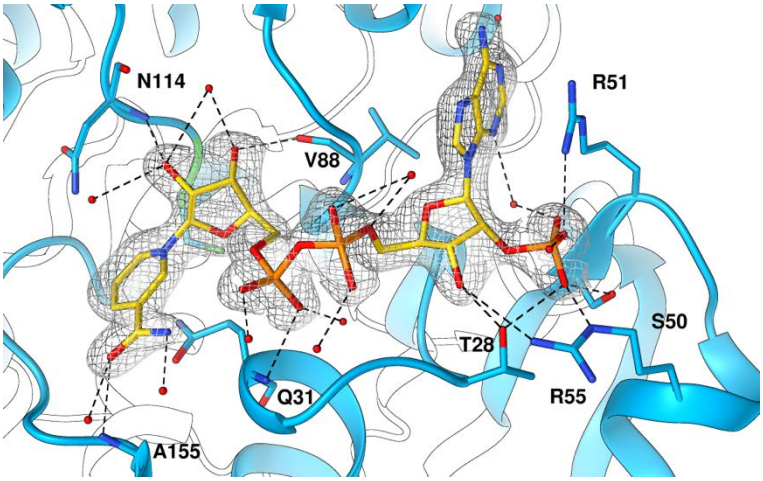


**Figure 6** Active site of Tfu-FNO in complex with NADP$^+$. Unbiased $2F_o - F_c$ electron density map calculated at 1.8 Å and contoured at 1.0 σ are drawn as grey chicken-wire. Potential hydrogen bonds are depicted with dashed lines and water molecules as red spheres. Residues in direct contact with NADP$^+$ are labeled. The orientation of the molecule is approximately 180° clockwise rotated along an axis perpendicular to the plane of the paper with respect to that in Figure 5. Color coding for atoms is as in Figure 5.

**Isolation and characterization of a thermostable $F_{420}$:NADPH oxidoreductase from *Thermobifida fusca***

Hemant Kumar, Quoc-Thai Nguyen, Claudia Binda, Andrea Mattevi and Marco W. Fraaije

*J. Biol. Chem. published online April 14, 2017*